Chinese Chemical Letters 33 (2022) 3823–3828

Contents lists available at ScienceDirect

Chinese Chemical Letters

journal homepage: www.elsevier.com/locate/cclet

Effective electrocatalytic hydrodechlorination of 2,4,6-trichlorophenol by a novel Pd/MnO_2/Ni foam cathode

Zi-Meng Zhang[a], Rui Cheng[a], Jun Nan[a], Xue-Qi Chen[a], Cong Huang[b], Di Cao[a], Cai-Hua Bai[a], Jing-Long Han[c], Bin Liang[c], Zhi-Ling Li[a,*], Ai-Jie Wang[a,c]

[a] State Key Laboratory of Urban Water Resource and Environment, School of Environment, Harbin Institute of Technology, Harbin 150090, China
[b] National Technology Innovation Center of Synthetic Biology, Tianjin Institute of Industrial Biotechnology, Chinese Academy of Sciences, Tianjin 300308, China
[c] State Key Laboratory of Urban Water Resource and Environment, School of Civil & Environmental Engineering, Harbin Institute of Technology Shenzhen, Shenzhen 518055, China

ARTICLE INFO

Article history:
Received 16 September 2021
Revised 24 October 2021
Accepted 23 November 2021
Available online 27 November 2021

Keywords:
Pd/MnO_2/Ni foam cathode
2,4,6-Trichlorophenol
Electrocatalytic hydrodechlorination
Dechlorination pathway
Atomic H* generation and utilization

ABSTRACT

Pd modified electrodes possess problems such as easy agglomeration and low electrolytic ability, and the use of manganese dioxide (MnO_2) to facilitate Pd reduction of organic pollutants is just started. However, there is still a limited understanding of how to match the Pd load and MnO_2 to realize optimal dechlorination efficiency at minimum cost. Here, a Pd/MnO_2/Ni foam cathode was successfully fabricated and applied for the efficient electrochemical dechlorination of 2,4,6-trichlorophenol (2,4,6-TCP). The optimal electrocatalytic hydrodechlorination (ECH) performance with 2,4,6-TCP dechlorination efficiency (92.58% in 180 min) was obtained when the concentration of $PdCl_2$ precipitation was 1 mmol/L, the deposition time of MnO_2 was 300 s and cathode potential was −0.8 V. Performance influenced by the exogenous factors (*e.g.*, initial pH and coexisted ions) were further investigated. It was found that the neutral pH was the most favorable for ECH and a reduction in dechlorination efficiency (6%~47.6%) was observed in presence of 5 mmol/L of NO_2^-, NO_3^-, S^{2-} or SO_3^{2-}. Cyclic voltammetry (CV) and quenching experiments verified the existence of three hydrogen species on Pd surface, including adsorbed atomic hydrogen (H^*_{ads}), absorbed atomic hydrogen (H^*_{abs}), and molecular hydrogen (H_2). And the introduction of MnO_2 promoted the generation of atomic H*. Only adsorbed atomic hydrogen (H^*_{ads}) was confirmed that it truly facilitated the ECH process. Besides H^*_{ads} induced reduction, the direct reduction by cathode electrons also participated in the 2,4,6-TCP dechlorination process. Pd/MnO_2/Ni foam cathode shows excellent dechlorination performance, fine stability and recyclable potential, which provides strategies for the effective degradation of persistent halogenated organic pollutants in groundwater.

2,4,6-Trichlorophenol (2,4,6-TCP) constitutes an important member of chlorinated organic compounds (COCs). 2,4,6-TCP has been widely applied as a pesticide precursor or formed during drinking water disinfection [1,2]. 2,4,6-TCP is toxic, durable, and resistant due to the existence of chlorine atomic [3]. Environmental risk of groundwater contamination by 2,4,6-TCP has raised great concerns due to its biotoxicity, persistence, and stability [4,5], urging the U.S. Environmental Protection Agency (EPA) to make it a priority pollutant [6].

Chemical remediation methods, especially chemical reduction, have been proposed as the most widely used method for detoxifying COCs due to their high efficiency [7]. Among chemical reduction, electrocatalytic hydrodechlorination (ECH) gains ever-growing interest due to its outstanding performance, mild reaction conditions, and convenient operation conditions [8], which has been regarded as a promising alternative in contamination control of COCs. In general, the mechanism of ECH can be summarized in two pathways: i) Direct reduction by direct electron transfer between pollutants and cathode surface [9]; ii) indirect reduction by atomic H* produced in process of water electrolysis [10]. Various previous studies have demonstrated that the latter way, ECH *via* atomic H*, is the dominant pathway for contaminant removal [11]. Details on the generation of atomic H* in the ECH process are elucidated as following (M represents metal catalyst and adsorbed atomic hydrogen is denoted as H^*_{ads}) (Eqs. 1-4) [12]:

$$H_2O + 2e^- + M \leftrightarrow 2H^*_{ads}M + 2OH^- \text{ (Volmer step)} \quad (1)$$

$$R\text{-}Cl + 2H^*_{ads}M \rightarrow 2M + R\text{-}H + H^+ + Cl^- \text{ (Dechlorination)}$$

* Corresponding author.
E-mail address: lzlhit@163.com (Z.-L. Li).

https://doi.org/10.1016/j.cclet.2021.11.068
1001-8417/

(2)

$$H^*_{ads}M + H_2O + e^- \rightarrow M + OH^- + H_2 \text{ (Heyrovsky step)} \quad (3)$$

$$H^*_{ads}M + H^*_{ads}M \rightarrow 2M + H_2 \text{ (Tafel step)} \quad (4)$$

Atomic H* plays a significant role in electrocatalytic hydrodechlorination [13], while hydrogen evolution reaction (HER), generating by both Heyrovsky step and Tafel step, consumes atomic H*, and inhibits ECH efficiency to some extent [14]. Considering this problem, many metals, such as Au [15], Pd [16], and Cu [17], serving as catalysts to modify the cathode surface, have been applied to strengthen the ECH process [18]. Among them, Pd has been proved as the most excellent one due to its good performance in atomic H* generation and storage *via* both H* adsorption on Pd surface (denoted as H^*_{ads}) and H* absorption into Pd crystal lattice forming Pd hydride (denoted as H^*_{abs}) [19]. However, since Pd is precious, expensive and easy-to-aggregation [20], its commercial application is limited.

To solve the Pd aggregation problem, Ni foam is introduced to improve Pd utilization by dispersing Pd particles due to its desirable 3D reticular structure [21]. Its high electrical conductivity accelerates electron transfer inside the Pd layer, which results in good reactivity [22]. Meanwhile, considering that Pd is inefficient in water electrolysis *via* the Volmer step [23], many transitional metal compounds have been induced to enhance atomic H* generation/retainment, such as nickel oxides [24], manganese oxides [25] Among them, MnO_2 with low cost has been proved as the most promising one to provide more atomic H* *via* water dissociation, which is favorable to be stored by Pd [26]. However, MnO_2 shows poor conductivity, and the excessive MnO_2 load inhibits both ECH and H_2 generation [23].

Recent studies have reported the introduction of MnO_2 to Pd/Ni foam cathode would enhance the production of atomic H* [26,27]. An appropriate amount of MnO_2 deposition is beneficial to enlarge the surface area of electrode and disperse Pd particles, while excessive MnO_2 can block the fold structure and reduce the conductivity, resulting in the inhabitation of ECH [28]. Thus, how to pair the dose of Pd and MnO_2 to enhance ECH was one of the focuses. Also, cathode potential is pivotal that determines both the amounts of electrons and catalytic activity, and how cathode potential regulation influences ECH performance by Pd and MnO_2 loaded electrode is largely unknown. Moreover, the influence of exogenous factors in the groundwater environment on catalytic activity, such as the initial pH and coexisted ions, still needs to be further explored.

Herein, a novel electrode was fabricated by introducing MnO_2 and Pd to the surface of Ni foam, aiming at improving ECH performance and reducing the dose of precious Pd. As a typical COC in groundwater, 2,4,6-TCP was selected as a target contaminant. Electrode operations (Pd load, MnO_2 load, and cathode potential) were optimized to seek the supervisor conditions for 2,4,6-TCP hydrodechlorination. Meanwhile, 2,4,6-TCP removal efficiency and kinetics, the proposed pathway as well as the impacts of environmental exogenous factors were thoroughly investigated to assess ECH performance by using Pd/MnO_2/Ni foam cathode (the detailed experimental content was given in the Supporting information).

Pd/MnO_2/Ni foam cathodes with the different Pd and MnO_2 loads were prepared, and the electrode under the preparation conditions of 1 mmol/L deposition solution concentration and 600 s electrodeposition time was selected for micro-characterization (Figs. S2A-C in Supporting information). SEM showed the morphology of 3D reticular structure at different magnification and found both MnO_2 and Pd were uniformly attached to the surface of foamed nickel electrode with cracks and grooves, indicating specific surface area was increased after deposition. Meanwhile, the elemental mapping of Pd/MnO_2/Ni foam confirmed the existence and uniform distribution of Ni, Pd, Mn and O (Figs. S2D and E in Supporting information). According to the elemental mapping, almost all MnO_2 were loaded on nickel foam skeleton, and a portion of Pd nano-particles covered on the MnO_2 layer, while the others dotted edges of the MnO_2 layer and the surface of Ni foam.

Subsequently, XRD pattern was performed to elucidate the formation of Pd phase (JCPDS No. 05–0681) with the characteristic diffraction peaks at $2\theta = 39.888°$ and 46.408° for Pd (111) and (200) [29], respectively (Fig. S2F in Supporting information). Moreover, three typical diffraction peaks of Ni (JCPDS No. 04–0850) were observed at $2\theta = 44.266°$, 51.618° and 76.157° corresponding to Ni (111), (200) and (220) [30], respectively. However, no significant characteristic diffraction peaks of MnO_2 were detected due to its slight crystallographic form [31], which might be concealed by others. Another possible explanation came from the fact that the intensities of Mn peaks would be more week after Pd loaded on the MnO_2 layer, which suggested that XRD could hardly detect the typical diffraction peaks of MnO_2. Nevertheless, the presence of Mn was proved by EDS and XPS, indicating the successful introduction of MnO_2.

After characterization, electrode operations that influenced ECH performance were investigated. Pd is a desirable catalyst for its excellent performance in atomic H* retainment, while SEM has shown that superfluous Pd nanoparticles lead to aggregation (Fig. S2 in Supporting information). Consequently, excessive Pd load resulted in a reduction in reactivity and ECH performance [23]. The effect of Pd load was investigated to find a chemical solution concentration required for the optimal dose (Fig. 1A). With the increase of Pd load, ECH efficiency of 2,4,6-TCP firstly increased from less than 5% to 89.21% and then decreased to 75.82%. The removal efficiency reached the optimal value of 89.21% when the concentration of sediment was 1 mmol/L. The electrocatalytic dechlorination followed pseudo-first-order kinetics. The reaction kinetic constant firstly increased to 11.37×10^{-3} min^{-1}, then decreased to 6.99×10^{-3} min^{-1}, and the reaction kinetic constant reached the maximum of 11.37×10^{-3} min^{-1} at 1 mmol/L (Fig. S4A, Table S1 in Supporting information). Moreover, cyclic voltammetry (CV) curves were conducted to illustrate the relationship between atomic H* and Pd load at a sweep rate of 1 mV/s (Fig. 1B). CV curves of different Pd loads showed two reduction peaks at −0.7 V and −0.2 V, which were probably assigned to H^*_{abs} and H^*_{ads} [26]. Pd load is positively correlated with atomic H production in a certain range. Moderate Pd load could store atomic H*, while excessive Pd load would cause aggregation and accelerate the formation of H_2 bubbles *via* a Heyrovsky or Tafel step [32]. This could explain the phenomenon for the reduction of dechlorination efficiency and kinetic rate at 2 mmol/L.

MnO_2 was introduced to expedite the generation of atomic H*, which could be absorbed into the Pd crystal lattice or adsorbed on the Pd surface. Since the incapability to store atomic H* of MnO_2, no significant dechlorination occurred without Pd load (Fig. 1A). ECH efficiency of 2,4,6-TCP firstly increased from 41.49% to 89.21% and then decreased to less than 5% with the increase of electrodeposition time of MnO_2 (Fig. 1C). The removal efficiency of 2,4,6-TCP of 300 s was 2.15 times higher than that of 0 s. Also, the reaction kinetic constant k of 300 s was 4.23 times higher than that of 0 s (Fig. S4B, Table S2 in Supporting information), indicating the improvement in generation of atomic H* after the load of MnO_2. Subsequently, electrochemical measurements including CV and LSV were applied to clarify the enhancement of atomic H* production. On the one hand, introducing MnO_2 to Pd/Ni foam made its hydrogen evolution potential positively rise from −0.8 V to −0.6 V (Fig. S5 in Supporting information), verifying the promotion of atomic H* generation *via* the Volmer step. On the other hand, two oxidation peaks were observed at around −0.7 V and −0.2 V (Fig. S5),

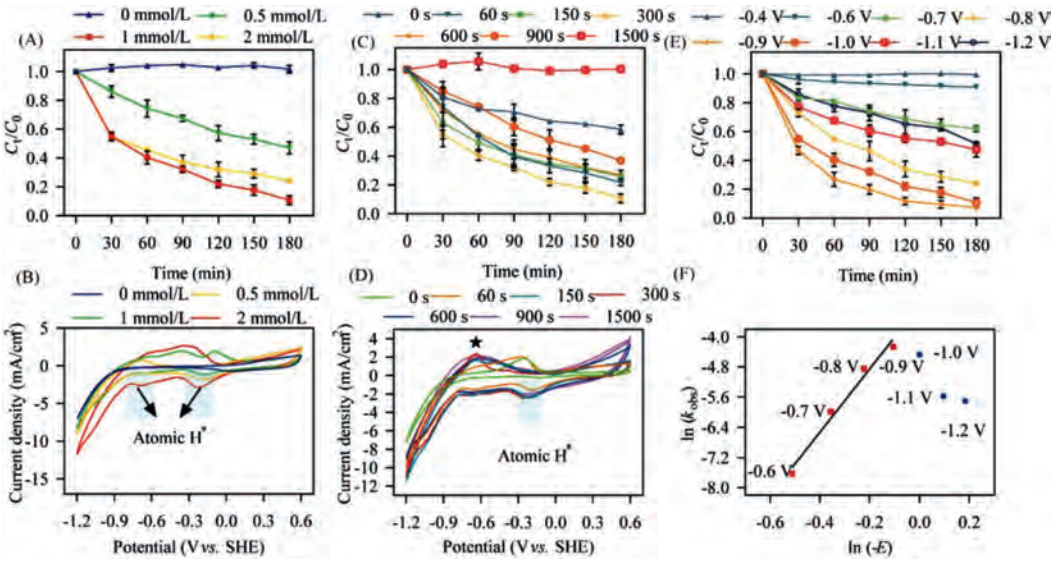

Fig. 1. ECH performance of Pd/MnO_2/Ni foam cathode at different (A) Pd loads, (C) MnO_2 loads, and (E) cathode potentials in N_2-saturated 0.1 mol/L Na_2SO_4 solution in the presence of 100 μmol/L of 2,4,6-TCP; Cyclic voltammograms recorded for Pd/MnO_2/Ni foam cathode under different (B) Pd loads and (D) MnO_2 loads at a sweep rate of 1 mV/s; and (F) the relationship between ln k_{obs} and ln($-E$) under different cathode potentials.

corresponding to the desorption of atomic H* adsorbed on (111) and (200) planes of polycrystalline Pd [27]. The peak current increased initially, and then reached its maximum (2.35 mA/cm^2) at 300 s (Fig. 1D), further verifying the promotion of water electrolysis by the addition of MnO_2. However, 2,4,6-TCP dechlorination rate and efficiency exhibited a drop trend as the electrodeposition time of MnO_2 exceeded 300 s (Fig. 1C). As previously reported, excessive MnO_2 would cause low electrical conductivity, which not only limited electron transfer but also inhibited the utilization of atomic H* [26]. This would be the major attribution for the decreased activity.

2,4,6-TCP dechlorination performance was investigated at cathode potentials from −0.4 V to −1.2 V by using the optimized Pd load (1 mmol/L) and MnO_2 load (300 s) (Fig. 1E). Dechlorination efficiency of 2,4,6-TCP increased from 0.51% to 92.58% when the potential decreased from −0.4 V to −0.9 V. Nevertheless, the sharp drop of dechlorination efficiency occurred as the cathode potential continued to fall to −1.2 V. The most effective potential was found to be −0.9 V, resulting in the dechlorination efficiency of 92.58%. Furthermore, kinetics analysis also obtained similar trends: the reaction kinetic constant reached the maximum of $14.07 \pm 1.25 \times 10^{-3}$ min^{-1} at −0.9 V (Fig. S4C, Table S3 in Supporting information), showing the optimized ECH performance at −0.9 V. Fig. 1F showed the relationship between ln k_{obs} and ln ($-E$), where k_{obs} indicated kinetics constant and E referred to the cathode potential. A linear relationship ($R^2 = 0.978$) was observed with potential ranging from −0.6 V to −0.9 V, and the apparent rate order was 8.40. The dechlorination efficiency was less than 10% with the potential of −0.4 V and −0.6 V because the non-Faraday current assisted adsorption process was the dominant process on the electrode surface rather than electron transfer. The improvement of ln k_{obs} at the potentials from −0.6 V to −0.9 V contributed to the enhancement of atomic H* generation, especially reactive H^*_{ads}, at the more negative potentials. However, considering that the hydrogen evolution reaction began to dominate around −0.9 V, the decrease in lnk_{obs} was attributed to the enhanced H_2 formation at the low potential, which competed with ECH and reduced utilization of atomic H*. Moreover, it also inhibited the effective electron and mass transfer at the liquid-catalyst interface.

The effects of the initial pH and coexisted ions on ECH performance were performed. The pH of catholyte plays a vital role in dechlorination reaction since the pathway of atomic H* formation

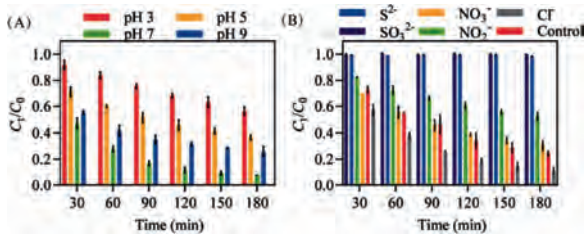

Fig. 2. Effects of (A) the initial pH and (B) the coexisted ions on 2,4,6-TCP removal performance by Pd/MnO_2/Ni foam cathode.

depends on the pH of the catholyte. The reaction equations that relied on pH are demonstrated as follows (Eqs. 5-8) [28]:

$$H_3O^+ + M + e^- \rightarrow M{-}H^* + H_2O \text{ (Acidic solution)} \quad (5)$$

$$M{-}H^* + H_3O^+ + e^- \rightarrow H_2 + M + H_2O \text{ (Acidic solution)} \quad (6)$$

$$M + H_2O + e^- \rightarrow M{-}H^* + OH^- \text{ (Neutral or alkaline solution)} \quad (7)$$

$$M{-}H^* + e^- + H_2O \rightarrow M + H_2 + OH^- \text{ (Neutral or alkaline solution)} \quad (8)$$

The initial pH influenced ECH performance was investigated as shown in Fig. 2A. With the initial pH of 3, 5, 7, and 9, the dechlorination efficiency approached 43.61%, 62.23%, 92.59%, and 74.21%, respectively. Although previous studies have confirmed the lower initial pH could provide more H^+ that favored HER process [26], 2,4,6-TCP is insoluble within the pH range of acidic condition ($pK_a = -5.99$) [33], which possibly causes the mass transfer limitation and decreases 2,4,6-TCP removal efficiency. With the increase of initial pH from 3 to 7, 48.98% higher dechlorination efficiency was achieved. On the one hand, HER was more inhabited by ECH, indicating the effective utilization of atomic H* went up. On the other, more amount of 2,4,6-TCP was dissolved, which could relieve the limitation of mass transfer. Consequently, a higher dechlorination efficiency was achieved with the increase of initial pH from 3

to 7. However, a decrease in reaction efficiency occurred with the increase of initial pH from 7 to 9, which was probably attributed to the shift in the dominant process of atomic H* production. Reactions of Eqs. 7 and 8 were dominant throughout the electrolysis at the initial pH of 9. Since Eq. 7 was much slower than Eq. 5, the generation of atomic H* was too slow to meet the normal need of ECH [34]. Above all, the pH of catholyte influenced ECH performance *via* regulating the competition between ECH and HER, and the optimized dechlorination efficiency was obtained at the condition with initial pH of 7.

Fig. 2B demonstrated the effects of coexisted ions (Cl^-, S^{2-}, SO_3^{2-}, NO_2^- and NO_3^-) on ECH performance by Pd/MnO_2/Ni foam cathode. The removal rate of 2,4,6-TCP with Cl^- was 1.17 times higher than that of control, suggesting that Cl^- worked as a redox medium that strengthened the electrochemical reduction process [35]. In comparison, the presence of S^{2-} and SO_3^{2-} completely inhibited the dechlorination process. Chen [36] confirmed that S^{2-} completely deactivated Pd catalytic activity even at a low concentration of 1.0 mmol/L. The inhibition of Pd catalytic activity by S^{2-} and SO_3^{2-} could be attributed to the competitive adsorption of HS^-, the change of electronic properties of Pd catalyst near sulfur atomic as well as the formation of Pd-S compound on the cathode surface [37]. NO_2^- also possessed a significant inhibitory effect on ECH, and the removal efficiency of 2,4,6-TCP decreased to 47.60%. It was probably caused by the competition of NO_2^- reduction for both electrons and atomic H* [20]. Moreover, NO_3^- showed a slight inhibition of dechlorination efficiency, and about 6% of decreased efficiency was obtained. This was because NO_3^- competed for the available atomic H* [38].

Electrocatalytic dechlorination mechanism and proposed pathway were determined by various methods. XPS spectra were conducted to reveal the physiochemical morphology of Pd and Mn in the Ni foam electrode before and after the dechlorination reaction (Fig. S6 in Supporting information). As shown in Fig. S6A, there were two pairs of spin-orbit components in both Pd 3d spectrum before and after 2,4,6-TCP dechlorination reaction, suggesting two valence states of Pd^0 and Pd^{2+} [16]. Characteristic peaks located at 337.39 eV and 342.69 eV were assigned to Pd^0 $3d_{5/2}$ and Pd^0 $3d_{3/2}$, while the binding energy of 339.09 eV and 345.59 eV represented Pd^{2+} $3d_{5/2}$ and Pd^{2+} $3d_{3/2}$, respectively. The binding energy of Pd^0 $3d_{3/2}$ and Pd^{2+} $3d_{5/2}$ showed a positive shift due to the changes in ligand environment around Pd atomics after the introduction of MnO_2 [39]. Pd^{2+} may come from the fact that oxygen vacancy cannot completely reduce Pd from divalent to zero or oxidation by O_2 [40]. The proportion of Pd in different valence states was changed during the reaction. Of these, the proportion of Pd^0 reduced from 86.49% to 42.53%, suggesting that partial Pd in electrode surface converted from Pd^0 to Pd^{2+}. A previous study confirmed that it was possibly caused by the formation of transitional Pd−Cl bond during dechlorination [13]. In our trials, excessive NaCl was added to better dissolve $PdCl_2$, resulting in the formation of Pd−Cl. Therefore, Pd^{2+} was likely to be derived from Pd−Cl formed during dechlorination reaction, the active site of which was provided by Pd^0. Note that Pd^{2+} could be reduced to Pd^0 at a cathode potential of −0.85 V, which suggested that this Pd/MnO_2/Ni foam cathode was renewable.

Fig. S6B (Supporting information) showed the XPS spectrum of Mn 2P before and after the reaction. Two characteristic peaks located at 642.01 eV and 653.80 eV were assigned to Mn $2p_{3/2}$ and Mn $2p_{1/2}$, suggesting Mn^{4+} acted as the dominating valence state of Mn [41]. The binding energy of Mn^{4+} $2p_{3/2}$ was shifted from 642.01 eV to 642.72 eV due to the fluctuation of Mn valence during the electrochemical dechlorination reaction, which was consistent with previous studies [23]. The intensities of Mn peaks after reaction were almost the same as the condition before reaction, indicating the stability and reusability of Mn. Furthermore, the stability of Pd/MnO_2/Ni foam cathode was evaluated by repeating the dechlorination process at −1.0 V for five cycles (Fig. S7 in Supporting information), which also proved the good stability and reusability.

Generally speaking, the electrocatalytic dechlorination mechanism included direct electron transfer and indirect reduction *via* atomic H*, thus it was necessary to clarify their specific contribution during 2,4,6-TCP dechlorination process. *t*-BuOH was served as a radical scavenger in quenching experiments due to its high reactivity with atomic H* [42]. As shown in Fig. 3A, the removal rate of TCP was inhibited from 47.70% to 23.30% when *t*-BuOH increased from 0 mmol/L to 500 mmol/L within 60 min, demonstrating the significant role of atomic H* during dechlorination process. The inset of Fig. 3A showed kinetic rate constants also decreased drastically with the increasing *t*-BuOH dose. Only 68.90% of kinetic rate constant without *t*-BuOH was obtained when *t*-BuOH was 500 mmol/L. The atomic H* is usually formed on the Pd surface *via* the interaction between hydrogen and the d orbital of Pd atom, which was proved by the change of Pd states in XPS analysis (Fig. S6A). Subsequently, the atomic H* attacked the C−Cl bond and made it cleavage. Nevertheless, the removal rate of 2,4,6-TCP with 500 mmol/L *t*-BuOH was still maintained at 87.09% after 180 min, suggesting the ECH performance was driven by both direct electron transfer and atomic H* reduction.

CV curves of Pd/MnO_2/Ni foam cathode with or without 2,4,6-TCP were conducted to identify the role of H^*_{ads} and H^*_{abs} in the dechlorination process of 2,4,6-TCP. Fig. 3B showed three oxidation peaks were located in potential ranges of −0.80 V to −0.60 V, −0.40 V to −0.20 V, and −0.20 V to −0.00 V assigning to H_2, H^*_{abs} and H^*_{ads}, respectively. The oxidation peak corresponding to H^*_{ads} disappeared after the addition of 2,4,6-TCP, indicating that H^*_{ads} was the key active hydrogen species, while H_2 and H^*_{abs} were negatively contributed to ECH.

To determine mechanistic insights into 2,4,6-TCP hydrodechlorination, we identified the electrolyzed intermediates by using GC–MS. Pd/MnO_2/Ni foam cathode generated detectable concentration of ion cluster for chlorophenols, for instance, 2,4-DCP, 2,6-DCP ($m/z = 161.96$), 2-CP, 4-CP ($m/z = 128.0$) as well as phenol ($m/z = 94.04$) (Fig. S8 in Supporting information). Based on GC–MS analysis results, the 2,4,6-TCP dechlorination pathway was proposed (Fig. 3C). Firstly, the *ortho* and *para*-Cl of 2,4,6-TCP were attacked by atomic H* to form 2,4-DCP and 2,6-DCP. Subsequently, as C−Cl was further attacked by atomic H*, both 2-CP and 4-CP were detected in MS analysis. It was noteworthy that 2-CP was maintained at a relatively higher concentration all along compared to 4-CP. This was because chemical reactions with lower Gibbs free energy and redox potential tended to occur [43]. As shown in Table S5 (Supporting information), when 2-CP was served as one of the products, reaction possessed the lower E and ΔG than 4-CP, while the opposite was true when it was applied as the reactant. It was likely to explain why 4-CP existed for a long time compared to 2-CP. Moreover, the dechlorination rates (R) of 2,4-DCP was in the order R(2-CP) > R(4-CP) due to the stereoscopic effect of orthochlorinated group [44]. Finally, phenol serving as the major end metabolite revealed the ECH process.

To summarize, Fig. 4 showed the schematic concept of the ECH reaction mechanism of 2,4,6-TCP by Pd/MnO_2/Ni foam cathode. In brief, the presence of MnO_2 enhanced the generation of atomic H*. The fate of atomic H* mainly included H^*_{ads}, H^*_{abs} and H_2, in which only H^*_{ads} participated in the hydrodechlorination process, while H^*_{abs} were inert, and H_2 inhibited the hydrodechlorination process. The introduction of MnO_2 strengthened the HO−H bond cleavage, resulting in the enhanced dechlorination activity by atomic H*. Both direct reduction and indirect reduction participated in the 2,4,6-TCP dechlorination process.

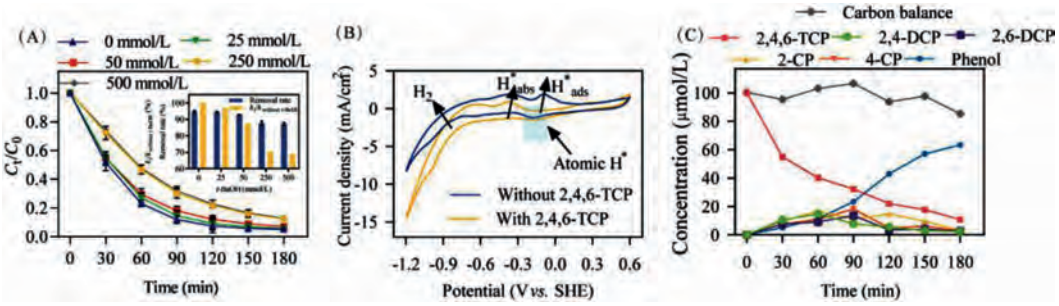

Fig. 3. (A) Quenching trials as a function of various *t*-BuOH concentrations. The inset showed the removal rates of 2,4,6-TCP with different *t*-BuOH concentrations and corresponding pseudo-first-order rate constants. (B) CV curves of Pd/MnO_2/Ni foam cathode with or without 2,4,6-TCP. (C) Time course of typical intermediates determined on Pd/MnO_2/Ni foam cathode at the cathode potential of −1.0 V.

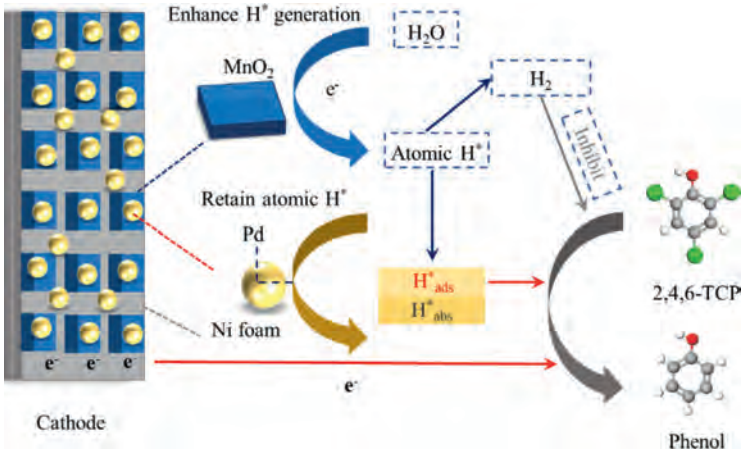

Fig. 4. Schematic concept of ECH reaction mechanism of 2,4,6-TCP by Pd/MnO_2/Ni foam cathode.

The Pd/MnO_2/Ni foam was successfully fabricated by using chemical deposition and electrodeposition methods, and the superior dechlorination activity of 2,4,6-TCP was obtained by optimizing Pd load, MnO_2 load and cathode potentials in our study. The introduction of MnO_2 enhanced the generation of atomic H*. Only H^*_{ads} were confirmed that truly facilitated the ECH process, and besides the reduction by H^*_{ads}, the direct reduction by cathode electrons also participated in the 2,4,6-TCP dechlorination process. As the major end metabolite, phenol revealed the ECH process. The highest ECH performance was obtained under the neutral condition and no significant inhibition was observed in presence of most common inorganic ions, representing the favorable application potential. This study gave strategies for the effective removal of persistent halogenated organic pollutants in groundwater.

Declaration of competing interest

We declare that we have no financial and personal relationships with other people or organizations that can inappropriately influence our work.

Acknowledgments

This study was supported by the NSFC-JSPS joint research program (No. 51961145202) and the Natural Science Foundation of Heilongjiang Province, China (No. C2018035).

Supplementary materials

Supplementary material associated with this article can be found, in the online version, at doi:10.1016/j.cclet.2021.11.068.

References

[1] P.M. Makinen, T.J. Theno, J.F. Ferguson, J.E. Ongerth, J.A. Puhakka, Environ. Sci. Technol. 27 (1993) 1434–1439.
[2] K. Zhu, C. Sun, H. Chen, et al., Chem. Eng. J. 223 (2013) 192–199.
[3] S. Oh, S. Chae, B.J. Kim, et al., RSC Adv. 8 (2018) 33980–33984.
[4] Y. Li, Y. Li, B. Jin, et al., Bioresour. Technol. 323 (2021) 124627.
[5] X.Q. Lin, Z.L. Li, B. Liang, et al., Water Res. 162 (2019) 236–245.
[6] L. Keith, W. Telliard, Environ. Sci. Technol. 13 (1979) 416–423.
[7] M. Sun, F. Yan, R. Zhang, et al., Environ. Sci. Technol. 44 (2010) 8209–8215.
[8] H.S. Yin, X.K. Cao, C. Lei, W.Q. Chen, B.B. Huang, ChemElectroChem 7 (2020) 1825–1837.
[9] B. Liu, H. Zhang, Q. Lu, G.H. Li, F. Zhang, Sci. Total Environ. 635 (2018) 1417–1425.
[10] G. Jiang, M. Lan, Z. Zhang, et al., Environ. Sci. Technol. 51 (2017) 7599–7605.
[11] R. Zhang, X. Wang, S. Yu, et al., Adv. Mater. 29 (2017) 1605502.
[12] Y. Wu, L. Gan, S. Zhang, et al., J. Hazard. Mater. 356 (2018) 17–25.
[13] A. Li, X. Zhao, Y. Hou, et al., Appl. Catal. B: Environ. 111-112 (2012) 628–635.
[14] Z. He, Q. Jian, J. Tang, et al., Electrochim. Acta 222 (2016) 488–498.
[15] L. Altamar, L. Fernández, C. Borras, et al., Sens. Actuators B 146 (2010) 103–110.
[16] X. Wei, X. Wan, J. Miao, et al., Catal. Lett. 149 (2019) 823–830.
[17] R. Mao, N. Li, H. Lan, et al., Environ. Sci. Technol. 50 (2016) 3829–3837.
[18] L.Z. Huang, S.U. Pedersen, E.T. Bjerglund, et al., Environ. Sci.: Nano 4 (2017) 2286–2296.
[19] B.P. Chaplin, M. Reinhard, W.F. Schneider, et al., Environ. Sci. Technol. 46 (2012) 3655–3670.
[20] J. Xu, L. Tan, S.A. Baig, et al., Chem. Eng. J. 231 (2013) 26–35.
[21] J.L. Lado, X. Wang, E. Paz, et al., ACS Catal. 5 (2015) 6503–6508.
[22] S.S. Raut, R. Shetty, N.M. Raju, S.P. Kamble, P.S. Kulkarni, Chemosphere 250 (2020) 126298.
[23] Y. Zhang, Z. Chen, L. Zhou, et al., J. Hazard. Mater. 369 (2019) 770–779.
[24] Y.F. Xu, M.R. Gao, Y.R. Zheng, J. Jiang, S.H. Yu, Angew. Chem. Int. Ed. 52 (2013) 8546–8550.
[25] X. Lu, J. Pan, E. Lovell, et al., Energy Environ. Sci. 11 (2018) 1898–1910.
[26] Z. Lou, J. Xu, J. Zhou, et al., Chem. Eng. J. 374 (2019) 211–220.
[27] Z.M. Lou, J.S. Zhou, M. Sun, et al., Chem. Eng. J. 352 (2018) 549–557.
[28] X. Wang, L. Chen, B. Dan, F. Wang, Int. J. Adv. Manuf. Technol. 94 (2018) 633–641.
[29] J. Li, H. Liu, X. Cheng, et al., Chem. Eng. J. 225 (2013) 489–498.
[30] H. Ma, Y. Xu, X. Ding, Q. Liu, C.A. Ma, Electrochim. Acta 210 (2016) 762–772.

[31] S. Devaraj, N. Munichandraiah, J. Phys. Chem. C 112 (2008) 4406–4417.
[32] H. Rong, S. Cai, Z. Niu, Y. Li, ACS Catal. 3 (2013) 1560–1563.
[33] C.J. Daughney, J.B. Fein, Environ. Sci. Technol. 32 (1998) 749–752.
[34] R. Subbaraman, D. Tripkovic, D. Strmcnik, et al., Science 334 (2011) 1256–1260.
[35] W.R. Leow, Y. Lum, A. Ozden, et al., Science 368 (2020) 1228–1233.
[36] M. Chen, S. Shu, J. Li, et al., J. Hazard. Mater. 389 (2020) 121876.
[37] X. Wei, X. Wan, Z. Sun, et al., ACS Omega 3 (2018) 5876–5886.
[38] G.V. Lowry, M. Reinhard, Environ. Sci. Technol. 35 (2001) 696–702.
[39] K. Wang, S. Shu, M. Chen, et al., Chem. Eng. J. 381 (2020) 122673.
[40] I.G. Casella, M. Contursi, J. Electroanal. Chem. 692 (2013) 80–86.
[41] A. Sanger, A. Kumar, A. Kumar, R. Chandra, Sens. Actuators B 234 (2016) 8–14.
[42] C. Liu, A.Y. Zhang, D.N. Pei, H.Q. Yu, Environ. Sci. Technol. 50 (2016) 5234–5242.
[43] A. Tang, L. Wang, R. Zhou, J. Mol. Struct. 960 (2010) 31–39.
[44] Z. Sun, X. Wei, Y. Han, S. Tong, X. Hu, J. Hazard. Mater. 244-245 (2013) 287–294.